Published in final edited form as:
Biochemistry. 2013 July 30; 52(30): 5103–5116. doi:10.1021/bi4005914.

N-terminal basolateral targeting signal unlikely acts alone for differential trafficking of membrane transporters in MDCK cells

Shiu-Ming Kuo[¥,§,*], **Li-Yuan Wang**[#¥], **Siyuan Yu**[#¥], **Christine E. Campbell**[§], **Sujith A. Valiyaparambil**[§], **Mark Rance**[†], and **Kenneth M. Blumenthal**[§]

[¥]Department of Exercise and Nutrition Sciences, University at Buffalo, Buffalo, NY 14214

[§]Department of Biochemistry, University at Buffalo, Buffalo, NY 14214

[†]Dept. of Molecular Genetics, Biochemistry and Microbiology, University of Cincinnati College of Medicine, Cincinnati, Ohio 45267

[#] These authors contributed equally to this work.

Abstract

We have shown previously, using confocal imaging and transport assays, that the N-terminus of the sodium-dependent vitamin C transporter 2 (SVCT2) can redirect apical SVCT1 to the basolateral membrane. Here, the SVCT model was used to further characterize the basolateral targeting peptide signal. Both the length (31 amino acids) and sequence accuracy of the SVCT2 N-terminus were found to be important in basolateral targeting activity, suggesting a structural requirement. However, the N-terminal basolateral targeting sequence did not appear to act alone, based on analyses of heterologous chimeras. Although diverse N-terminal basolateral targeting signals from multi-pass membrane proteins can all redirect apical protein from the same gene family to the basolateral membrane, none of the N-terminal basolateral targeting signals can redirect the TM and C-terminus regions from a different gene family. Instead, the presence of these heterologous N-terminal basolateral targeting signals affected the trafficking of otherwise apical protein, causing their accumulation in a stable tubulin-like non-actin structures. Non-targeting N-terminal sequences had no effect. Similar protein retention was observed previously and in this study when the C-terminus of apical or basolateral protein was mutated. These results suggest that the N- and C-termini interact, directly or indirectly, within each gene family for basolateral targeting. CD and 2D NMR analyses both found a lack of regular secondary structure in the conserved SVCT2 N-terminus, consistent with the presence of partner(s) in the targeting unit. Our finding, a departure from the prevailing single peptide motif model, is consistent with the evolution of basolateral transporters from the corresponding apical genes. The interaction among the N-terminus, its partner(s) and the cellular basolateral targeting machinery needs to be further elucidated.

[*]**Corresponding Author**: To whom correspondence should be addressed. Telephone: (716)829-5664. Fax: (716)829-3700. smkuo@buffalo.edu..

Author Contributions

All authors have given approval to the final version of the manuscript.

Supporting Information.

The cross-species alignments of N-terminal basolateral targeting sequences of AQP3, SLC6a2 and SLC13a3 are shown in Figure 1S. The results of peptide purification for the structure analysis are summarized in Figure 2S. The alignment of the C-termini of each gene family, SVCT, AQP, SLC6, and SLC13, is shown in Figure 3S. Table 1S shows the pI of N- and C-termini of basolaterally and apically targeted transporter pairs. This material is available free of charge via the Internet at http://pubs.acs.org.

No competing financial interests have been declared.

Vectorial transport of nutrients and metabolites is an important function of polarized epithelial cells in multi-cellular organisms. To fulfill this need, multi-pass membrane transporters are differentially targeted to the apical and basolateral membranes. The importance of correct targeting is demonstrated by the existence of several genetic diseases in which membrane proteins in epithelial cells are incorrectly sorted (1). The focus of our research is to characterize the peptide sequence mediating the basolateral targeting and to understand its mechanism of its action. While the differential targeting of single-pass membrane receptors has been examined previously to some extent, little information is available for the targeting of multi-pass membrane transporters such as our model, sodium-dependent vitamin C transporters (SVCT), which are predicted to have both N- and C-termini in the cytosol (2).

Our previous publications analyzed the pair of homologous yet differentially targeted monomeric transporters, human SVCT1 and SVCT2 (SLC23A1 and SLC23A2) (3, 4). SVCT1 localizes in the apical membrane of well-differentiated intestinal and renal epithelial cells while SVCT2 localizes in the basolateral membrane of the same cells. Using deletion mutagenesis, we showed that SVCT1 lacking its N-terminal sequence still localized to the apical membrane. The N-terminal sequence of SVCT1 also could not redirect SVCT2 to the apical membrane based on our analyses of homologous chimeras between SVCT1 and SVCT2. In contrast, we found that the N-terminal sequence of SVCT2 was able to redirect SVCT1 to the basolateral membrane with ELMAI as the critical residues involved in the targeting. A brief summary of SVCT2 sequences that possess basolateral targeting activity is shown in Figure 1A. Consistent with our conclusion based on SVCT1 and SVCT2, a newly characterized SLC23 family member, SLC23A4 (sodium-dependent nucleobase transporter), does not have the ELMAI motif and is apically localized in MDCK cells (5).

The conclusion of an N-terminal basolateral-targeting signal in SVCT2 was consistent with observations made on three other membrane transporters, mouse aquaporin-3 water channel (AQP3), human solute carriers (SLC) 6A2, and SLC13A3 (6-8). For each transporter, an N-terminal basolateral-targeting signal was identified. Similar to SVCT2, the targeting signal was able to redirect a protein of the same gene family to the basolateral membrane: AQP3 redirected AQP2, SLC6A2 redirected SLC6A3, and SLC13A3 redirected SLC13A2. Interestingly, besides the presence of critical hydrophobic residues in all cases, there is no apparent homology in the primary sequences of the basolateral targeting signals from the four gene families but the signals are evolutionarily conserved across species within each gene family (4)(Figure 1S, Supporting Information).

In the literature, a basolateral-targeting signal has often been referred to as a dileucine motif or tyrosine motif. However, it is evident that by themselves these widely present hydrophobic amino acids cannot mediate basolateral targeting but may represent a critical site for protein-protein interaction (9). In the case of SVCT2, of the predicted 99 amino acids in its N-terminus (Figure 1A, sequence 1), an ELMAI motif was critical for basolateral targeting. Nontheless, 15 SVCT2 N-terminal amino acid residues including ELMAI in the middle (Figure 1A, sequence 5) was not sufficient to redirect SVCT1 to the basolateral membrane (4). This length requirement is consistent with our hypothesis that similar to many other biological processes, basolateral targeting is achieved by protein/protein interaction. Because the N-terminus of SVCT2 is conserved across species, it is also expected that a sequence unique to SVCT2 is preferentially needed for the basolateral targeting. In the first part of the work presented here, the length and sequence-fidelity requirement of the basolateral-targeting signal in SVCT2 were further addressed by analyzing additional homologous chimeras.

The protein/protein interaction for basolateral targeting can be achieved in at least two possible ways: the N-terminal signal by itself provides the necessary secondary structure essential for the interaction with the cellular machinery; or the basolateral targeting requires an interaction between the N-terminal signal and other sequence(s) in the protein to achieve the functional targeting unit. Examination of these two possible modes of action has never been reported and represented another goal of our study. As presented and discussed below, our observations made on heterologous chimeras and the results of our peptide structure analysis contribute to the understanding of the complicated basolateral-targeting process.

EXPERIMENTAL PROCEDURES

Materials

L-[carboxyl-^{14}C]ascorbic acid (13 mCi/mmol) (CFA.620) and L-ascorbic acid (A-5960) were purchased from Amersham Biosciences (Buckingshire, England) and Sigma Aldrich (St. Louis, MO), respectively. All cell culture reagents were from Invitrogen Corp. (Carlsbad, CA) except characterized fetal bovine serum, which was purchased from Hyclone, USA (Logan, UT). All other chemicals used were of reagent grade. Primers used for the mutagenesis; the construction of expression plasmids; and the sequencing were from Operon Biotechnologies, Inc. (Huntsville, AL) (Table 1). The sequences of the parent EGFP-tagged proteins, hSVCT1-EGFP and hSVCT2-EGFP, were previously published (4).

Plasmid preparation and the generation of stable cell lines expressing SVCT proteins and chimeric protein containing SVCT sequence

QuikChange Site-Directed Mutagenesis Kits from Stratagene (La Jolla, CA) and Fennzymes Phusion Site-Directed Mutagenesis Kits from New England Biolabs (Ips-wich, MA) were used for all N- or C-terminal SVCT mutations following the manufacturers' protocols. pT-REx-DEST30-based plasmid containing hSLC11a2v2 cDNA sequence was a gift from Dr. Michael Garrick of the University at Buffalo (10). hSLC11a2v2 sequence was cloned into pEGFP-N2 plasmid, the same parental plasmid used to construct pSVCT1-EGFP and pSVCT2-EGFP, by restriction digest and ligation at the NheI and ApaI sites to form pSLC11a2v2. The 18 amino acid peptide, DNEDT**ELMAI**YTTENGLA, that included the critical SVCT2 N-terminal basolateral-targeting sequence ELMAI, was then cloned into pSLC11a2v2 immediately after the initiation methionine using restriction digest and ligation at the NheI site. The new plasmid was designated as pSVCT2(50-67)-SLC11a2v2. The transformation of *E. Coli* (DH5α) for colony expansion; the transfection of MDCK cells for stable expression; and the verification of successful transfection of plasmids were carried out following our published protocols (4). All primer sequences are included in Table 1. The sequencing of plasmids and PCR products from MDCK cellular DNA extract was performed to confirm the intended mutation and stable transfection in MDCK cells, respectively, by Roswell Park Cancer Institute (Buffalo, NY).

Confocal fluorescence microscopy, total monolayer fluorescence measurement and uptake assays of MDCK cells stably expressing various plasmids

All experiments were performed on early passages of MDCK cells stably transfected with various plasmids. Unless indicated otherwise, these cells were used for experiments at 14-17 days after seeding. Cells used for imaging experiments were grown on the Lab-Tek II chambered cover glasses (Nalge Nunc International Naperville, IL) as described previously (3). Confocal images were captured in the Confocal and 3-D Imaging Core Facility of the University at Buffalo using a Zeiss LSM510 Meta System in conjunction with a Pecon 37 °C Heating Insert. The confocal image acquisition and data analysis were carried out following our published protocols (4). No adjustments of brightness, contrast, sharpness, etc. were made to any of the acquired live cell images. Images shown were representative of

multiple cell images acquired from multiple chambers of cells. Total live-cell fluorescence emission from stably-transfected MDCK cells grown in the 96-well plates was also measured using Biotek Synergy HT Multi-Detection Microplate Reader following our published protocol (4). Ascorbate uptake assays were performed on cells grown on 6-well plates (to measure the accumulation through the apical membrane) or on Transwell permeable supports (Corning Inc, Corning, NY) (to measure accumulation through the apical and basolateral membranes separately) following our published protocols (4). The efficiency of membrane incorporation in Figures 2, 3, 5, and 8 was determined by normalized total ascorbate uptake, i.e. a ratio between total uptake from apical and basolateral sides (a measurement of functional membrane incorporation) and total monolayer EGFP fluorescence (a measurement of protein expression).

Confocal fluorescence microscopy of stably-transfected MDCK cells stained with phalloidin and DAPI

After the medium removal and PBS rinsing, stably-transfected MDCK cells were fixed with 100% ice-cold HPLC-grade methanol for 5 minutes at 4° C. We have previously determined that methanol fixation as described did not lead to appreciable loss of EGFP fluorescence (unpublished observation). Fixed cells were then incubated with 20% normal goat serum and 0.1% Triton X-100 in PBS for 2 hours at room temperature to block any non-specific binding. Alexa Fluor 568 phalloidin (Invitrogen) solution was then applied following manufacturer's instruction to stain for F-actin (11) at room temperature for 60 minutes. For 4′,6-diamidino-2-phenylindole, dihydrochloride (DAPI) staining of double strand DNA, Slowfade Gold antifade reagent with DAPI (Invitrogen) was added to the monolayer after blocking without further incubation. Fluorescence confocal imaging was all performed on freshly processed samples in the same UB confocal facility as for the live cell imaging. EGFP imaging was performed using 488 nm excitation and 500-550 nm emission filter. A 561 nm laser was used to excite Alexa Fluor 568 and paired with an emission filter of 575-615 nm. Two-photon laser illumination was applied to produce excitation (around 350 nm) suitable to produce emission from DAPI-stained samples, and an emission filter of 390-465 nm was used to acquire images. Experiments with wildtype MDCK cells showed that duo-color imaging did not affect the results of phalloidin and DAPI staining (unpublished observation). Images were captured as 0.46 μm slices and ~25 slices were collected for well-differentiated MDCK cells. No adjustments of brightness, contrast, sharpness, etc. were made to any of the images except for the purpose of 3D analysis in Figure 7B.

Construction of His-tagged hSVCT2 N-terminus-expressing plasmids and peptide purification

The N-terminal sequence of hSVCT2 (N13-89) (Figure 1B) was PCR amplified from pSVCT2-EGFP and cloned into a pJS18-based plasmid (12) between EcoRI and HindIII sites to produce protein for circular dichroism (CD) analysis. Fennzymes Phusion Site-Directed Mutagenesis Kit was then used to add 10 more N-terminal residues from hSVCT2 (N90-99) (Figure 1B) for the purpose of 2D NMR. PCR primers used for the construction of expression plasmids are included in Table 1 and the plasmids were sequenced by the facility at the Roswell Park Cancer Institute (Buffalo, NY). The peptide expressed in *E. coli* (DH5α) contained, in tandem, maltose-binding protein (MBP), His8-tag, TEV protease cleavage site, enterokinase cleavage site, and SVCT2 N13-89 or SVCT2 N13-99. Published protocols (12) with minor modifications were followed for the culture of *E. Coli*; the peptide extraction and purification on Ni^{+2}-column; the enterokinase cleavage; and HPLC purification. Briefly, because the expressed peptide was soluble, the 10,000×g supernatant after French press was loaded directly onto a Ni^{+2}-column pre-equilibrated with 20 mM imidazole, and 300 mM imidazole was used for the elution of His-tagged protein. The eluted protein was

concentrated using Amicon Ultra (MWCO 10K) before dialysis. After overnight enterokinase treatment the peptide of interest was purified by ammonium sulfate precipitation followed by a second Ni^{+2}-column to remove the undigested protein and MBP-His8 fragment. The final HPLC purification of hSVCT2-N13-89 and hSVCT2-N13-99 was performed on an Alltech Prosphere 300 C4 column (5 μ, 250 mm) with a 20%-60% buffer B step-gradient (Buffer A: 0.1% trifluoroacetic acid, Buffer B: 75% acetonitrile, 0.1% trifluoroacetic acid, flow rate: 1 ml/min). A Beckman Coulter System Gold 166 Detector at 220 nm was used to follow the appearance of the peptide of interest from the HPLC column. The expected molecular weights of the peptides are 8.3 kDa (N13-89) and 9.5 kDa (N13-99) (Figure 1B), and were observed in 14% SDS gel comparing to lysozyme (14 kDa) and aprotinin (6.5 kDa). The molecular weight of the peptide was further confirmed by MALDI-TOF MS (matrix-assisted laser desorption ionization time-of-flight mass spectrometry) (13).

Structural analysis of the hSVCT2 N-terminus using circular dichroism (CD) spectroscopy and 2D nuclear magnetic resonance (NMR)

CD analysis was performed with a JASCO (Easton, MD) J-715 Spectrometer with 25 μg and 100 μg peptide/ml 5 mM sodium phosphate buffer, pH 6.9 following a published protocol (13). The spectrum obtained from the 100 μg/ml sample and its high tension voltage (HT) curve during the spectrum acquisition have been submitted to the Protein Circular Dichroism Data Bank (PCDDB) (PCDDB ID #CD0004076000). NMR studies were performed on the hSVCT2 N-terminus (13-99) peptide (0.5 mM) in 90% H_2O/10%D_2O, pH 7.0, at 295K. Data were collected at 600MHz on an Agilent Inova spectrometer. Two-dimensional homonuclear 2Q COSY (14, 15) and ^{1}H-^{15}N FHSQC (16) (^{15}N at natural abundance) experiments were performed, and the data was processed with NMRPipe (17) and analyzed with Sparky (18).

RESULTS

Chimeric proteins between truncated or mutated N-terminal sequence of SVCT2 and SVCT1

The SVCT2-SVCT1 chimeric model that we have published (4) was used (Figure 2A model). We have shown previously that SVCT1 protein without its own N-terminus is functionally localized in the apical membrane (Figure 1, sequence 4)(4) and thus is a good model to test the basolateral targeting activity of the SVCT2 N-terminal sequence. An SVCT2 sequence including 66 residues encompassing the critical ELMAI is sufficient to redirect SVCT1 to the basolateral membrane (Figure 1, sequence 3) but a shorter insertion of ELMAI-containing sequence with only 15 residues cannot (Figure 1, sequence 5)(4). It is possible that a longer SVCT2 N-terminal sequence is needed in order to stabilize a specific secondary structure involved in basolateral targeting. Alternatively, the 15-residue peptide failed in the basolateral targeting perhaps because of being too close to the start of the TM region. If the latter were the case, then the addition of non-specific spacer amino acids after the 15 residues should restore basolateral targeting. Experiments were designed to distinguish between these two possibilities and the results are shown in Figures 2 and 3.

Lengthened native SVCT2 N-terminal sequences (20-31 amino acids) were examined for their basolateral targeting ability. Adding 5 SVCT2 N-terminal residues before the 15 amino acids (construct 45-64, Figure 2A) did not change the apical localization of the chimera (Figure 2B,C), consistent with our previous finding that the absence of residues 45-48 did not alter the basolateral targeting by the SVCT2 N-terminus (Figure 1, sequence 3)(4). Eight additional SVCT2 N-terminal residues after the 15 amino acids (construct 50-72, Figure 2A) led to more basolateral incorporation based on an increased uptake of ascorbate from the basolateral side of the Transwell (Figure 2D). Adding 5 more SVCT2 N-terminal residues

before the 23 amino acids (construct 45-72, Figure 2A) had a similar effect on basolateral incorporation (Figure 2B, 2D). In the last construct in Figure 2 where 16 amino acids from SVCT2 after residue 60 were added (construct 50-80, Figure 2A), the EGFP-tagged protein became predominantly basolaterally localized based on the results of both confocal imaging (Figure 2B) and Transwell uptake experiments (Figure 2D). Overall, the longer SVCT2 N-terminal sequence led to more efficient basolateral membrane incorporation (Figure 2E). Based on the results in Figure 2, we concluded that around 30 residues from the N-terminus of SVCT2 is sufficient for basolateral targeting and the sequence 3′ to the critical ELMAI appears more important. This is complementary to our previous finding that the deletion of residues 1-48 did not affect the basolateral localization (Figure 1, sequences 2-3) (4).

After we established the peptide length requirement, additional experiments were conducted to determine whether the length requirement can be explained by a need for spacer between the critical ELMAI and the TM.

In Figure 3, four SVCT mutant constructs were analyzed. Each one had residues 50-64 followed by a SVCT2-related sequence (Figure 3A). None of the proteins from these constructs appeared completely basolateral (Figure 3B) although all of them showed more uptake activity from the basolateral side compared to the apical side in Transwell experiment (Figure 3C). When the membrane incorporation was analyzed by comparing total uptake to the total fluorescence of the monolayer (Figure 3E), constructs with the longer but deranged/mutated N-termini (50-64+69-79w and 50-64+69-77AAAA) actually showed less membrane incorporation, judging from the ratio between total uptake and total fluorescence (Figure 3D). It is clear that length per se cannot promote basolateral targeting. This result is inconsistent with the simple spacer requirement hypothesis. Instead, the conserved SVCT2 N-terminal sequence probably has structural significance.

Heterologous chimeric proteins with various N-terminal basolateral targeting sequences

A different chimera approach was also taken to distinguish between the functional significance of a longer peptide and a simple requirement for spacer between the critical residues ELMAI and the TM (Figure 4). In this experiment, the SVCT2 basolateral targeting sequence was included in the N-terminus of an unrelated multi-pass membrane transporter, SLC11A2v2 (Figure 4A). In Figure 4B, two SLC11A2v2 constructs, SLC11A2v2 and SVCT2(50-67)-SLC11A2v2 were compared. SLC11A2v2 is known to be apically expressed in enterocytes (19). Confocal imaging of SLC11A2v20 supports its predominantly apical localization in well-differentiated MDCK cells (Figure 4B, left panels). Despite the lengthy N-terminus of SLC11A2v2 (70 amino acids (20)) that could serve as spacer (Figure 4A), N-terminal insertion of SVCT2(50-67) including the critical ELMAI did not efficiently redirect SLC11A2v2 to the basolateral membrane (Figure 4B, right panels). Nevertheless, when the right and left panels of Figure 4B were compared, it is evident that the N-terminal insertion of SVCT2(50-67) did change the apparent protein distribution of SLC11A2v2. Unlike SLC11A2v2, SVCT2(50-67)-SLC11A2v2 was also present intracellularly including forming fluorescent tubulin-like structure (TLS) (21, 22) across the cell (Figure 4B, top right panel). Because this construct, like all others that we have used, had EGFP trailing the C-terminus (Figure 4A), fluorescent protein found along TLS likely represented full-length protein with EGFP. EGFP by itself or EGFP-tagged protein with TM defects were found distributed throughout the cytosol (3, 4, 23). Overall, this result and that of our SVCT chimeras in Figure 3 consistently support the conclusion that a longer peptide is needed, likely due to functional significance instead of the requirement of spacer to the TM region.

We have also inserted other known basolateral-targeting signals into the N-terminus of SVCT1 similar to the experiment in Figures 2 and 3 (Figure 5A). There were two purposes for carrying out this set of heterologous chimera experiments: to examine the prevailing

hypothesis that the N-terminal basolateral targeting sequence alone is sufficient for functional interaction with the cellular machinery in basolateral targeting; and to determine whether the fluorescent TLS observed in SVCT2(50-67)-SLC11A2v2 was simply due to a foreign sequence in the protein. If the first hypothesis is true, basolateral targeting signal should be functional independent of the TM and C-terminal sequences. Thus, heterologous N-terminal basolateral targeting sequence from a different gene family should work as well. If fluorescent TLS was simply a result of foreign sequence insertion into the N-terminus, all heterologous chimeras should display this feature.

The schematic presentation of the chimeras and N-terminal sequences that we used for the heterologous chimera constructs are listed in Figure 5A. Of them, AQP3, SLC13A3 and SLC6A2 are basolateral proteins (6-8). Similar to SVCT (4), the N-termini of these three proteins are highly conserved (Figure 1S, Supporting Information). The N-termini of AQP3 and SLC13A3 are nearly 100% conserved across the species while the longer SLC6A2 N-terminus is overall 70% conserved but 100% conserved in the region where critical residues for basolateral targeting were identified.

Among our chimeras, AQP3_27 has the entire N-terminus of AQP3 but AQP3_20 and AQP3_27 both have the critical residues for basolateral targeting (residues in grey box in Figure 5A). Neither AQP3_20 nor AQP3_27 were in the basolateral membrane (Figure 5B, C). The presence of the basolateral targeting signal, nevertheless, affected the localization of otherwise apical SVCT1-EGFP. Confocal images of these two chimeras showed fluorescent TLS as well similar to that observed with SVCT2(50-67)-SLC11A2v2. Again, the membrane incorporation efficiency was low as shown by a low ratio of total uptake to the total fluorescence (Figure 5D), and greater residual transport activity was found in the apical membrane (Figure 5C). These observations of AQP3_20 and AQP3_27 cannot simply be a result of foreign amino acid sequence. AQP2_14 contained the entire N-terminus of apical protein AQP2 (8) yet showed normal apical localization in confocal imaging as parental SVCT1 and no TLS. The uptake results of AQP2_14 were also similar to that of parental apical SVCT1 (Figure 5B, C, D compared to (4, 24)).

SLC13A3_15 had the entire N-terminus of the basolateral protein SLC13A3 and its localization was similar to that of AQP3_20 and AQP3_27 (Figure 5B, C, D) including the fluorescent TLS (Figure 5B). SLC6A2_15 has a short segment of the N-terminus of SLC6A2 with only part of the critical basolateral targeting signals (7). Similar to the parental SVCT1, SLC6A2_15 was apically localized in confocal images and showed abundant transport activity from the apical side (Figure 5B, C). More importantly, the heterologous chimera showed little fluorescent TLS (Figure 5D). In contrast, SLC6A2_29, including a longer peptide with all basolateral targeting signals of SLC6A2 (7), showed more intracellular localization including TLS (Figure 5B); less membrane incorporation (Figure 5D); and residual apical ascorbate transport activity (Figure 5C).

Figure 5E examined the protein distribution pattern of SLC13A3_15 in subconfluent MDCK cells. These cells were flatter than fully differentiated MDCK cells enabling an observation of the xy fluorescence more clearly. They were also rapidly dividing, a different stage compared to the well-differentiated MDCK cells used in the rest of the study. The fluorescence distribution of SLC13A3_15 was different from that of SVCT1 or SVCT2 in subconfluent MDCK cells (3). Instead, the protein localized in discrete perinuclear regions of the cells and in TLS (Figure 5E).

Because all heterologous chimeras with complete basolateral targeting sequences showed a similar phenotype, i.e. lack of basolateral presence and instead in TLS, we considered it

unlikely that N-terminal sequence alone is sufficient for the cellular machinery in the targeting event.

Characterization of linear EGFP structure in heterologous chimeric proteins

The fluorescent TLS in Figures 4 and 5 appeared to have a uniform width around 0.5-0.6 μm. This width was close to the optical resolution of the microscope so the actual structure could be thinner. The consistency of the structure, the estimated width, and the magnitude of fluorescence made it unlikely that these lines resulted from randomly distributed protein.

To determine the stability of the fluorescent TLS, we exposed the cells to 25% osmolarity hypotonic shock. After 44 minutes, the TLS remained mostly intact (Figure 6 right panel compared to left panel). During this period, some cells became deformed (Figure 6 right panel arrows). The zones of darkness between the cells that were barely visible initially broadened (Figure 6 right panel compared to left panel). However, neither of these changes affected the TLS, which did not migrate into the deformed area (follow arrows in Figure 6 right panel).

We also found that neither the appearance of the TLS nor membrane fluorescence was affected by cell fixation with 100% ice-cold methanol. This stability enabled co-localization analysis as shown in Figure 7. In Figure 7A, co-localization of EGFP-tagged protein with nuclei was determined. For basolaterally localized construct 50-80, the partially basolateral protein 50-64+69-72, and the apical protein SLC6A2_15, fluorescence was found outside the nuclei (Figure 7A). For SLC13A3_15, in addition to the fluorescence found surrounding the nuclei, the fluorescent TLS seemed to traverse nuclei (Figure 7A). To determine whether the TLS went through nuclei, random areas were enlarged and 3D reconstructed. The color of nuclei was converted to red in ImageJ for better contrast to the green fluorescence (Figure 7B). By comparing the top and bottom sets of Figure 7B, it was apparent that the surface of the nuclei was not smooth and TLS simply passed through the creases along the outside of the nuclei but did not invade the nuclei.

Cytoskeleton has been proposed to be involved in the protein trafficking (25) and apical localization (26, 27). The localization of F-actin in well-differentiated MDCK cells was then determined by phalloidin labeling. F-actin was only found in the cell peripheries (Figure 7C). Some overlap of F-actin with TLS at the cell periphery may exist but it was difficult to resolve. Overall, the TLS and F-actin showed different distribution patterns.

C-terminal deletion mutation of chimeric proteins

In our previous characterization of SVCT targeting signals, we concluded that the C-terminal sequence is important for membrane localization of both apical and basolateral multi-pass membrane proteins (4). When apical or basolateral SVCT chimeras with the C-terminus of SVCT2 were mutated at a critical region of the C-terminus, all chimeras showed a similar phenotype as the heterologous chimeras in Figures 4 and 5: fluorescent TLS, low membrane incorporation, and more residual ascorbate uptake from the apical side (4). In the present study, chimeras with the C-terminus of SVCT1 were mutated at the corresponding critical region of the C-terminus (Figure 8A). For the apically localized (50-64) (4) and basolaterally localized (50-80) chimeras (Figure 2), this deletion similarly led to the appearance of a widespread fluorescent TLS (Figure 8B). In addition, poor efficiency in membrane incorporation (Figure 8D) with more residual apical ascorbate uptake (Figure 8C) was observed. SLC13A3_15 displayed TLS and poor ascorbate uptake (Figure 5B-D), and its C-terminal mutant had the same profile (Figure 8B-D). The consistent observations made in two studies, one using a mutated C-terminus of SVCT1 (this study) and one previously with a mutated C-terminus of SVCT2 (4), further supported an indispensable role of the C-

terminus in both apical and basolateral membrane targeting of multi-pass membrane proteins such as SVCT.

Structural analysis of N-terminus of SVCT2

Studies on SVCT chimeras (Figures 2 and 3) demonstrated the preference of a specific SVCT2 N-terminal 31-residue sequence for basolateral targeting activity and thus suggested the presence of a unique higher order structure in this region to interact with the cellular targeting machinery. Results from several types of heterologous chimeras (Figures 4 and 5), on the other hand, suggested that the N-terminal signal by itself was not sufficient for the basolateral targeting. One possible explanation that reconciles the two sets of observations is that the protein structure necessary for the basolateral targeting requires an interaction between the N-terminus and other part(s) of the protein that are conserved within each gene family. If this were true, the basolateral targeting N-terminus of SVCT2 would not necessarily have an intrinsic structure when analyzed alone. To analyze the intrinsic structure of the N-terminus of SVCT2, the N-terminus of SVCT2 was expressed and purified (Figure 2S, Supporting Information for purification results). The peptides expressed were longer than the sequence needed for the biological targeting activity to maximize the possibility to detect the structure (Figure 1 for sequences expressed comparing to the sequences needed for basolateral targeting).

With the excellent solubility of the SVCT2 N-terminus peptide in the biological buffer, we were able to take two approaches for the structural analysis of the N-terminus: CD and solution NMR with unlabeled peptide.

The far UV CD spectrum of the peptide is shown in Figure 9. With a HT cut-off at 900 V (Figure 9A), we obtained a spectrum between 196-250 nm. A lack of Δε peaks at both concentrations (Figure 9B) suggested a low probability for α-helix (28). Although the CD spectrum predicted the peptide to have a moderate probability of ß-turns (28%), it considered the peptide to be mostly unordered structure (60%).

Representative 2D spectra recorded for the NMR analysis are shown in Figure 10. The amide proton region of a 2Q COSY spectrum is shown in the left panel and a ^{1}H-^{15}N HSQC spectrum is shown in the right panel. The experiments had adequate spectral resolution with most resonances being clearly resolved. The modest dispersion of the amide protein chemical shifts did not support the significant presence of stable secondary structure. The heterogeneity of the resonance peak intensities indicated a possible heterogeneity in the dynamic properties of the peptide.

The results of CD and NMR analyses consistently indicated little likelihood of intrinsic structure in the N-terminal basolateral targeting sequence of SVCT2. This, similar to the observation made on heterologous chimeras, does not favor the current model that the N-terminus acts alone in the basolateral targeting.

DISCUSSION

There were two substantive findings in the paper: possible N- and C-terminal cooperation in basolateral targeting, and intracellular protein localization forming a stable TLS. Neither one has been reported in the area of differential targeting of membrane proteins in epithelial cells. Although these findings were made by observing C-terminal EGFP-tagged proteins in live cells, they are most likely physiologically relevant based on our previous comparison of natural and EGFP-tagged SVCTs (3); and a global consistency between the results from immunofluorescence and fluorescentprotein tagging experiments (29).

The need for a hydrophobic motif in basolateral targeting has been widely accepted for some time but the nature of the signal has not been characterized in detail in multi-pass membrane transporters such as SVCT with both N- and C-termini in the cytosol. We previously identified 5 critical residues, ELMAI, in the N-terminus of SVCT2 for its basolateral targeting (4). In this study, we found that residues downstream from the ELMAI seem to be more important in this regard (Figure 2). A 31-residue peptide, including 5 residues upstream and 21 residues downstream of ELMAI (Figure 2A), can redirect SVCT1 to the basolateral membrane similar to the full length N-terminus of SVCT2 (Figure 2). We showed the importance of sequence fidelity and thus the downstream sequence served more than as a spacer between the basolateral targeting signal and the TM (Figures 2, 3, 4). For example, construct 50-72 (Figure 2) was better in basolateral targeting than 50-64+69-77AAAA (Figure 3) although the latter had a longer N-terminus. A requirement for sequence fidelity is consistent with the evolutionary conservation of the entire N-terminus of SVCT2.

The length and fidelity requirement of the SVCT2 basolateral targeting signal supported the involvement of a particular peptide structure in the basolateral targeting. There are, however, two possible ways for the N-terminal sequence to contribute to the structure needed for the basolateral targeting: an intrinsic structure in the N-terminus that would be sufficient for the basolateral targeting; or an induced structure when the N-terminus meets its partner(s) during the targeting event. We examined the two possibilities by using two approaches: a biological targeting test and peptide structure determination.

Heterologous chimeras between known N-terminal basolateral targeting sequences and SVCT1 were used in the biological targeting test (Figure 5). AQP3, SLC6A2 and SLC13A3 are from two distinct super-groups of proteins, major intrinsic proteins and solute carriers. All three have basolateral targeting signals in their N-termini and were able to redirect apical protein within their own gene family to the basolateral membrane (6-8). If these N-termini can act independently in basolateral targeting, we would expect them to direct apical proteins from other gene families to the basolateral membrane. As shown in Figure 5, all three N-terminal basolateral targeting signals failed to redirect apical SVCT1 to the basolateral membrane (Figure 5). Thus, results from the biological targeting test do not favor the possible presence of an intrinsic structure in the N-terminus that is sufficient for the basolateral targeting.

Structural information for N-terminal basolateral targeting signal was not available for any membrane protein. To differentiate between two possible modes of action by the N-terminal basolateral targeting sequence, we undertook in vitro expression of the SVCT2 N-terminus and performed CD and NMR analyses. The SVCT2 N-terminus turned out to be low in regular secondary structure based on both analyses (Figures 9, 10). Results from the peptide structural analysis therefore also do not favor the possible presence of an intrinsic structure in the N-terminus that is sufficient for the basolateral targeting.

The results of our experimental structure analysis are consistent with the results of protein structure prediction. Both PredictProtein (http://www.predictprotein.org) and Predictor of Natural Disordered Regions (http://www.pondr.com) predicted that the SVCT2 N-terminal peptides we used for our experiments (Figure 1B) as well as the entire N-terminus of SVCT2 are significantly disordered in structure (over 60%). The critical residues for basolateral targeting ELMAI are in a region that was predicted to be disordered. The N-termini of SVCT2, AQP3, SLC6A2 and SLC13A3 do not share similarity in primary sequence and have wide range of pI from 3.9 to 12 (Table S1). Yet using the two softwares mentioned above, we found that the N-terminus of SLC6A2 (62 amino acids) was also mostly disordered. Similar to SVCT2, the critical residues for basolateral targeting in

SLC6A2 were predicted to be in regions that are disordered. AQP3 N-terminus at 27 residues and SLC13A3 N-terminus at 15 residues are too short for structure prediction and likely too short for stable helical formation. The N-terminal basolateral targeting sequences are not the only functionally important and conserved peptides with no defined structure. Disordered regions have been found in other evolutionary conserved sequences. They were shown to mediate protein-protein interaction (30) and are important players in various cellular events (31).

If the N-terminus needs to meet its partner(s) during the basolateral-targeting event, with what intramolecular sequence might the N-terminal basolateral targeting signal collaborate with? Circumstantial evidence and available data point to the C-terminus. For multi-pass membrane transporters, existing evidence supports the localization of both N- and C-termini in the cytosolic side making an interaction between N- and C-termini topologically feasible. When an N-terminal sequence with basolateral targeting activity was inserted into an apical protein from another gene family, the apical localization was perturbed (Figures 4, 5), yielding a phenotype similar to what we have observed when the C-termini of SVCTs were mutated (4)(Figure 8). In addition, while the C-termini of the four groups of membrane transporters, SVCT, AQP, SLC6, SLC13, are highly conserved within each gene family with 45-51% identity and 56-61% homology (Figure 3S, Supporting Information), alignments of the C-termini from different gene families yielded no significant similarity. Our suggestion of collaboration between N- and C-termini is an advancement from our previous conclusion that the N- and C-termini are both required for the basolateral targeting (4). It is possible that while a “perfect” N- and C-terminal collaboration, as seen in the wildtype transporter family pairs, leads to the basolateral targeting, the perturbed collaboration occurring in heterologous chimeras or when the C-terminus of a basolateral protein was mutated, not only leads to failure in the basolateral targeting but also prevents the C-terminus from performing efficient apical targeting. However, our current knowledge cannot differentiate between the two possible modes of collaboration: a direct physical contact between the N- and C-termini after membrane insertion; or an interaction between the two termini only in the presence of cellular machinery involved in the basolateral targeting. In our view, the latter mode is more likely. Because N- and C-terminal interaction may hinder the transport function, it should be an event reserved for the moment of differential targeting.

Our N- and C-terminal interaction model could also explain, based on protein evolution, why N-terminal basolateral targeting signals from different gene families, although functionally conserved, do not share sequence homology (Figure 1 and 5 to compare four different basolateral targeting signals). Apical proteins are more ancient evolutionarily because single cell organisms only have the environmental facing apical membrane (32). The need for separate basolateral proteins in each gene family likely arises later to meet the needs of multicellular organisms. As a result, N-terminal basolateral targeting signal probably evolved within each gene family to fulfill the need for interaction with the C-terminus. With the wide range of pI in N- and C-termini (Table 1S, Supporting Information), it is unlikely that the charge acts as a determining factor in the interaction. The N- and C-terminus each has some critical hydrophobic amino acid residues that are probably important for protein-protein interaction during the basolateral targeting (9). Interestingly, the lengths of the N- and C-terminus follow the same order among these four groups of membrane transporters in that SVCT>SLC6>SLC13 ≈ AQP.

Although the TLS observed by our lab has not been previously reported, it cannot simply be an artifact. The structure was stable (Figures 6, 8) and there were no other apparent cellular changes in these stably transfected MDCK cells. MDCK cells expressing various heterologous chimeras that we have characterized in Figures 4 and 5 divided and formed monolayers similarly. None of their Transwell experiments detected increased paracellular

leak (results not shown). This was also not a random event. Heterologous N-terminal basolateral targeting sequences affected the apical localization of SVCT1 with consistent phenotype of fluorescent TLS along with poor membrane incorporation and more residual apical transport activity (Figures 4, 5). Foreign N-terminal sequences that do not have the complete basolateral targeting signal, such as the N-terminus of AQP2 and 15 residues from SLC6A2, did not affect SVCT1 apical localization or transport activity (Figure 5). The linear structure was not observed when EGFP alone was expressed or when the TM was truncated (4, 23). Proteins that failed the quality control of endoplasmic reticulum have not been reported to line up in TLS (33-38). Although actin is known to be involved in the differential targeting of membrane proteins (26, 27), these lines did not co-localize with F-actin (Figure 7C). Vesicle movement along microtubules has been previously demonstrated (25, 39) and microtubule motors were shown to be involved in the transport of single-pass membrane receptors (40-42).

In conclusion, our research contributes to the understanding of the pathway for membrane transporter differential targeting in epithelial cells. Our results indicate that while the membrane insertion of transporters is known to be co-translational, the differential targeting of multi-pass plasma membrane transporters to the apical or basolateral membrane is most likely not a cotranslational event as was previously shown for intracellular membrane proteins (43). Both apical and basolateral targeting require the contribution of the C-terminus of the protein, and changes in either the N- or C-terminus can lead to similar protein retention in a stable intracellular post-Golgi structure. The concept of a cellular post-Golgi decoding machinery for the differential targeting has been previously introduced (1). Although we did not examine the interaction between the code and the decoding machinery, our results indicated that the code for the basolateral targeting is unlikely to be a single peptide motif as currently believed.

Supplementary Material

Refer to Web version on PubMed Central for supplementary material.

Acknowledgments

We appreciate the technical guidance and input of Dr. Wade Sigurdson, Director of Confocal and 3-D Imaging Facility of the University at Buffalo, especially in the interpretation of the tubulin-like structure and the 3-D image analysis. We thank Sathy V. Balu-Iyer and Vandana Iyer of the University at Buffalo in providing access and assistance in CD analysis. We also thank the insight of Dr. Murray Ettinger of the University at Buffalo in the protein structure data interpretation.

Funding Sources

Funding was provided partially through NIH grants R01GM063855 to M. R., and RR19077 and RR027755 to the UC College of Medicine NMR facility.

ABBREVIATIONS

CD	circular dichroism
DAPI	4′,6-diamidino-2-phenylindole, dihydrochloride
HT	High-tension voltage
MBP	maltose-binding protein
NMR	nuclear magnetic resonance
SLC	Solute Carrier

SVCT	sodium-dependent vitamin C transporter
TLS	tubulin-like structure
TM	transmembrane domain

REFERENCES

1. Mellman I, Nelson W. Coordinated protein sorting, targeting and distribution in polarized cells. Nat Rev Mol Cell Biol. 2008; 9:833–845. [PubMed: 18946473]
2. Tsukaguchi H, Tokui T, Mackenzie B, Berger UV, Chen XZ, Wang Y, Brubaker RF, Hediger MA. A family of mammalian Na+-dependent L-ascorbic acid transporters. Nature. 1999; 399:70–75. [PubMed: 10331392]
3. Boyer JC, Campbell CE, Sigurdson WJ, Kuo S-M. Polarized localization of vitamin C transporters, SVCT1 and SVCT2, in epithelial cells. Biochem. Biophys. Res. Commun. 2005; 334:150–156. [PubMed: 15993839]
4. Varma S, Sobey K, Campbell CE, Kuo S-M. Hierarchal contribution of N- and C-terminal sequences to the differential localization of homologous sodium-dependent vitamin C transporters, SVCT1 and SVCT2, in epithelial cells. Biochemistry. 2009; 48:2969–2980. [PubMed: 19216494]
5. Yamamoto S, Inoue K, Murata T, Kamigaso S, Yasujima T, Maeda J, Yoshida Y, Ohta K, Yuasa H. Identification and functional characterization of the first nucleobase transporter in mammals: implication in the species difference in the intestinal absorption mechanism of nucleobases and their analogs between higher primates and other mammals. J Biol Chem. 2010; 285:6522–6531. [PubMed: 20042597]
6. Bai X, Chen X, Feng Z, Hou K, Zhang P, Fu B, Shi S. Identification of basolateral membrane targeting signal of human sodium-dependent dicarboxylate transporter 3. J Cell Physiol. 2006; 206:821–830. [PubMed: 16331647]
7. Gu H, Wu X, Giros B, Caron M, Caplan M, Rudnick G. The NH(2)-terminus of norepinephrine transporter contains a basolateral localization signal for epithelial cells. Mol Biol Cell. 2001; 12:3797–3807. [PubMed: 11739781]
8. Rai T, Sasaki S, Uchida S. Polarized trafficking of the aquaporin-3 water channel is mediated by an NH2-terminal sorting signal. Am J Physiol Cell Physiol. 2006; 290:C298–304. [PubMed: 16135541]
9. Bogan A, Thorn K. Anatomy of hot spots in protein interfaces. J Mol Biol. 1998; 280:1–9. [PubMed: 9653027]
10. Garrick M, Kuo H, Vargas F, Singleton S, Zhao L, Smith J, Paradkar P, Roth J, Garrick L. Comparison of mammalian cell lines expressing distinct isoforms of divalent metal transporter 1 in a tetracycline-regulated fashion. Biochem J. 2006; 398:539–546. [PubMed: 16737442]
11. Chazotte B. Labeling cytoskeletal F-actin with rhodamine phalloidin or fluorescein phalloidin for imaging. Cold Spring Harb Protoc 2010. 2010 pdb.prot4947.
12. Smith J, Alphy S, Seibert A, Blumenthal K. Differential phospholipid binding by site 3 and site 4 toxins. Implications for structural variability between voltage-sensitive sodium channel domains. J Biol Chem. 2005; 280:11127–11133. [PubMed: 15632158]
13. Seibert A, Liu J, Hanck D, Blumenthal K. Arg-14 loop of site 3 anemone toxins: effects of glycine replacement on toxin affinity. Biochemistry. 2003; 42:14515–14521. [PubMed: 14661964]
14. Braunschweiler L, Bodenhausen G, Ernst RR. Analysis of networks of coupled spins by multiple quantum N.M.R. Mol Phys. 1983; 48:535–560.
15. Rance M, Chazin W, Dalvit C, Wright P. Multiple-quantum nuclear magnetic resonance. Methods Enzymol. 1989; 176:114–134. [PubMed: 2811682]
16. Mori S, Abeygunawardana C, O'Neil Johnson M, van Zijl P. Improved sensitivity of HSQC spectra of exchanging protons at short interscan delays using a new fast HSQC (FHSQC) detection scheme that avoids water saturation. J Magn Reson B. 1995; 108:94–98. [PubMed: 7627436]
17. Delaglio F, Grzesiek S, Vuister G, Zhu G, Pfeifer J, Bax A. NMRPipe: a multidimensional spectral processing system based on UNIX pipes. J Biomol NMR. 1995; 6:277–293. [PubMed: 8520220]

18. Goddard, TD.; Kneller, DG. SPARKY 3. University of California; San Francisco: 2008.
19. Montalbetti N, Simonin A, Kovacs G, Hediger M. Mammalian iron transporters: Families SLC11 and SLC40. Mol Aspects Med. 2013; 34:270–287. [PubMed: 23506870]
20. Czachorowski M, Lam-Yuk-Tseung S, Cellier M, Gros P. Transmembrane topology of the mammalian Slc11a2 iron transporter. Biochemistry. 2009; 48:8422–8434. [PubMed: 19621945]
21. Bellett G, Carter J, Keynton J, Goldspink D, James C, Moss D, Mogensen M. Microtubule plus-end and minus-end capture at adherens junctions is involved in the assembly of apico-basal arrays in polarised epithelial cells. Cell Motil Cytoskeleton. 2009; 66:893–908. [PubMed: 19479825]
22. Quinones G, Danowski B, Devaraj A, Singh V, Ligon L. The posttranslational modification of tubulin undergoes a switch from detyrosination to acetylation as epithelial cells become polarized. Mol Biol Cell. 2011; 22:1045–1057. [PubMed: 21307336]
23. Karim-Jimenez Z, Hernando N, Biber J, Murer H. Molecular determinants for apical expression of the renal type IIa Na+/Pi-cotransporter. Pflugers Arch. 2001; 442:782–790. [PubMed: 11512035]
24. Varma S, Campbell CE, Kuo S-M. Functional role of conserved transmembrane segment 1 residues in human sodium-dependent vitamin C transporters. Biochemistry. 2008; 47:2952–2960. [PubMed: 18247577]
25. Soldati T, Schliwa M. Powering membrane traffic in endocytosis and recycling. Nat Rev Mol Cell Biol. 2006; 7:897–908. [PubMed: 17139330]
26. Lebreton S, Paladino S, Zurzolo C. Selective roles for cholesterol and actin in compartmentalization of different proteins in the Golgi and plasma membrane of polarized cells. J Biol Chem. 2008; 283:29545–29553. [PubMed: 18701450]
27. Antalffy G, Caride A, Pászty K, Hegedus L, Padanyi R, Strehler E, Enyedi A. Apical localization of PMCA2w/b is enhanced in terminally polarized MDCK cells. Biochem Biophys Res Commun. 2011; 410:322–327. [PubMed: 21672522]
28. Hammes, G. Spectroscopy for the biological sciences. John Wiley & Sons, Inc.; Hoboken, New Jersey: 2005.
29. Stadler C, Rexhepaj E, Singan V, Murphy R, Pepperkok R, Uhlén M, Simpson J, Lundberg E. Immunofluorescence and fluorescent-protein tagging show high correlation for protein localization in mammalian cells. Nat Methods. 2013; 10:315–323. [PubMed: 23435261]
30. Sivakolundu S, Nourse A, Moshiach S, Bothner B, Ashley C, Satumba J, Lahti J, Kriwacki R. Intrinsically unstructured domains of Arf and Hdm2 form bimolecular oligomeric structures in vitro and in vivo. J Mol Biol. 2008; 384:240–254. [PubMed: 18809412]
31. Nguyen Ba A, Yeh B, van Dyk D, Davidson A, Andrews B, Weiss E, Moses A. Proteome-wide discovery of evolutionary conserved sequences in disordered regions. Sci Signal. 2012; 13:rs1. [PubMed: 22416277]
32. Mostov K, Apodaca G, Aroeti B, Okamoto C. Plasma membrane protein sorting in polarized epithelial cells. J Cell Biol. 1992; 116:577–583. [PubMed: 1730769]
33. Cheng S, Gregory R, Marshall J, Paul S, Souza D, White G, O'Riordan C, Smith A. Defective intracellular transport and processing of CFTR is the molecular basis of most cystic fibrosis. Cell. 1990; 63:827–834. [PubMed: 1699669]
34. Yamamoto K, Fujii R, Toyofuku Y, Saito T, Koseki H, Hsu V, Aoe T. The KDEL receptor mediates a retrieval mechanism that contributes to quality control at the endoplasmic reticulum. EMBO J. 2001; 20:3082–3091. [PubMed: 11406585]
35. Ellgaard L, Helenius A. Quality control in the endoplasmic reticulum. Nat Rev Mol Cell Biol. 2003; 4:181–191. [PubMed: 12612637]
36. Lilley B, Ploegh H. Multiprotein complexes that link dislocation, ubiquitination, and extraction of misfolded proteins from the endoplasmic reticulum membrane. Proc Natl Acad Sci U S A. 2005; 102:14296–14301. [PubMed: 16186509]
37. Anelli T, Sitia R. Protein quality control in the early secretory pathway. EMBO J. 2008; 27:315–327. [PubMed: 18216874]
38. Zaarour N, Demaretz S, Defontaine N, Mordasini D, Laghmani K. A highly conserved motif at the COOH terminus dictates endoplasmic reticulum exit and cell surface expression of NKCC2. J Biol Chem. 2009; 284:21752–21764. [PubMed: 19535327]

39. Sheetz M, Vale R, Schnapp B, Schroer T, Reese T. Movements of vesicles on microtubules. Ann N Y Acad Sci. 1987; 493:409–416. [PubMed: 3109300]
40. Lafont F, Burkhardt J, Simons K. Involvement of microtubule motors in basolateral and apical transport in kidney cells. Nature. 1994; 372:801–803. [PubMed: 7997271]
41. Xue X, Jaulin F, Espenel C, Kreitzer G. PH-domain-dependent selective transport of p75 by kinesin-3 family motors in non-polarized MDCK cells. J Cell Sci. 2010; 123:732–741.
42. Hirokawa N, Noda Y, Tanaka Y, Niwa S. Kinesin superfamily motor proteins and intracellular transport. Nat Rev Mol Cell Biol. 2009; 10:682–696. [PubMed: 19773780]
43. Saksena S, Shao Y, Braunagel S, Summers M, Johnson A. Cotranslational integration and initial sorting at the endoplasmic reticulum translocon of proteins destined for the inner nuclear membrane. Proc Natl Acad Sci U S A. 2004; 101:12537–12542. [PubMed: 15306686]
44. Subramanian VS, Marchant JS, Boulware MJ, Said HM. A carboxy-terminal region dictates the apical plasma membrane targeting of the human sodium-dependent vitamin C transporter-1 in polarized epithelia. J. Biol. Chem. 2004; 279:27719–27728. [PubMed: 15084584]
45. Gasteiger, E.; Hoogland, C.; Gattiker, A.; Duvaud, S.; Wilkins, MR.; Appel, RD.; Bairoc, A. Protein Identification and Analysis Tools on the ExPASy Server. In: Walker, JM., editor. The Proteomics Protocols Handbook. Humana Press; Totowa, New Jersey: 2005. p. 571-607.

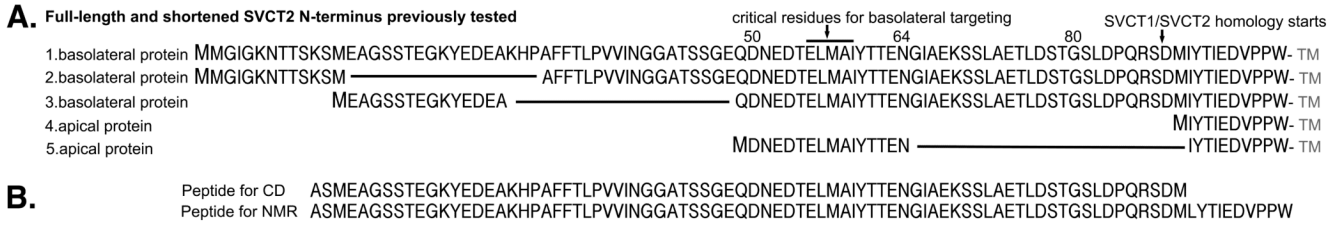

FIGURE 1.

hSVCT2 N-terminal sequences that (A) were tested previously for basolateral targeting biological activity (4) and (B) were analyzed for secondary structure in this study.

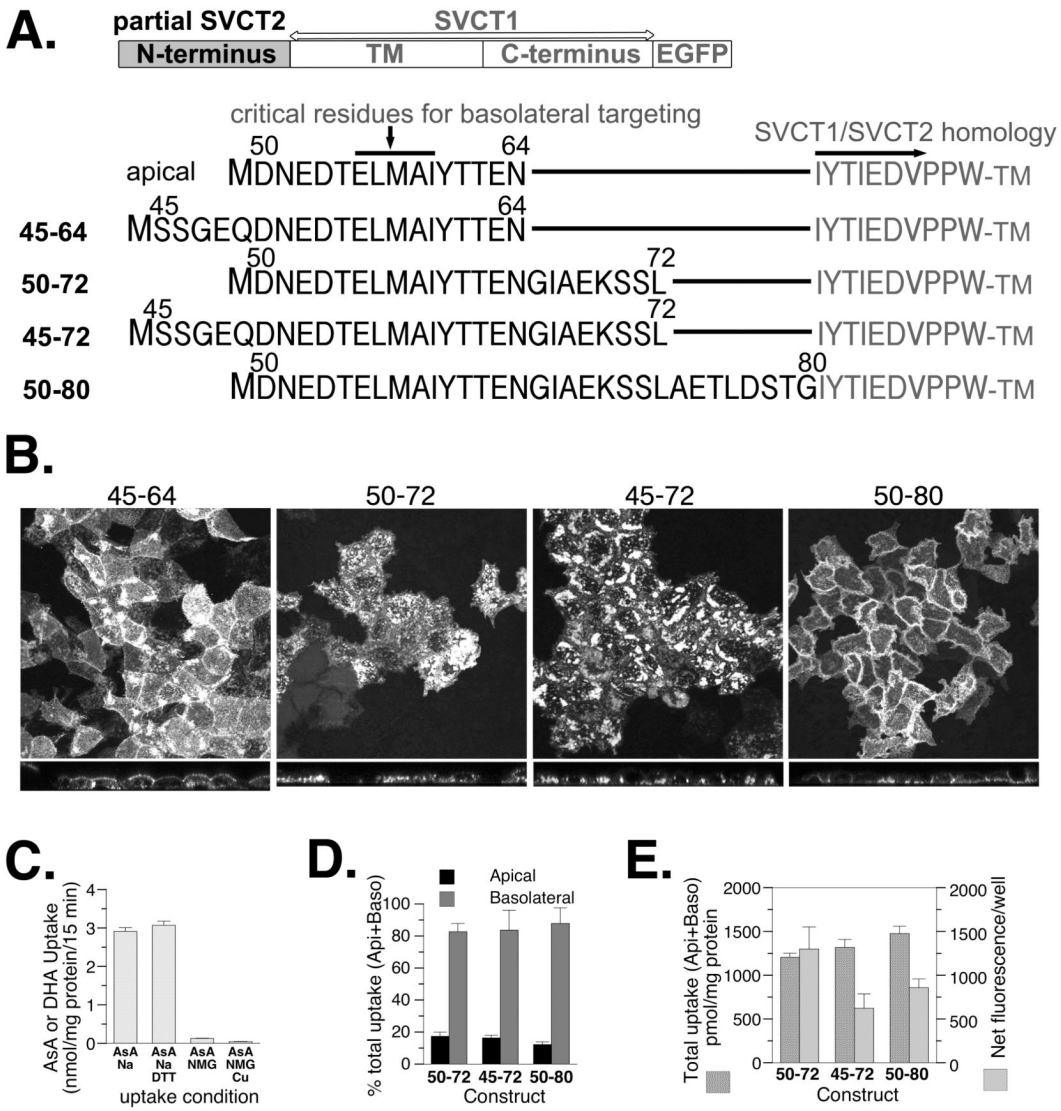

FIGURE 2.

The effects of length and residue position of SVCT2 N-terminal sequence in its ability to target SVCT1 to the basolateral membrane of well-differentiated MDCK cells. (A) Schematic and sequence presentation of homologous chimeras containing SVCT2-specific N-terminal sequences linking to SVCT1 sequence without any SVCT1-specific N-terminal sequence. (B) Representative confocal merged XY and YZ images of MDCK cells stably expressing each construct. (C) MDCK cells stably expressing construct 45-64 were grown on the 6-well plate and the uptake of vitamin C, ascorbate (AsA) and its oxidized form dehydroascorbate (DHA), across the apical membrane was measured. (D) The proportion of ascorbate uptake across the apical (Api) and basolateral (Baso) membrane of MDCK cells stably expressing each construct and grown on Transwells. (E) The efficiency with which each construct was incorporated into the cell membrane. (C,D,E) Data shown are means±SD of triplicate wells. Some error bars are too small to be visible.

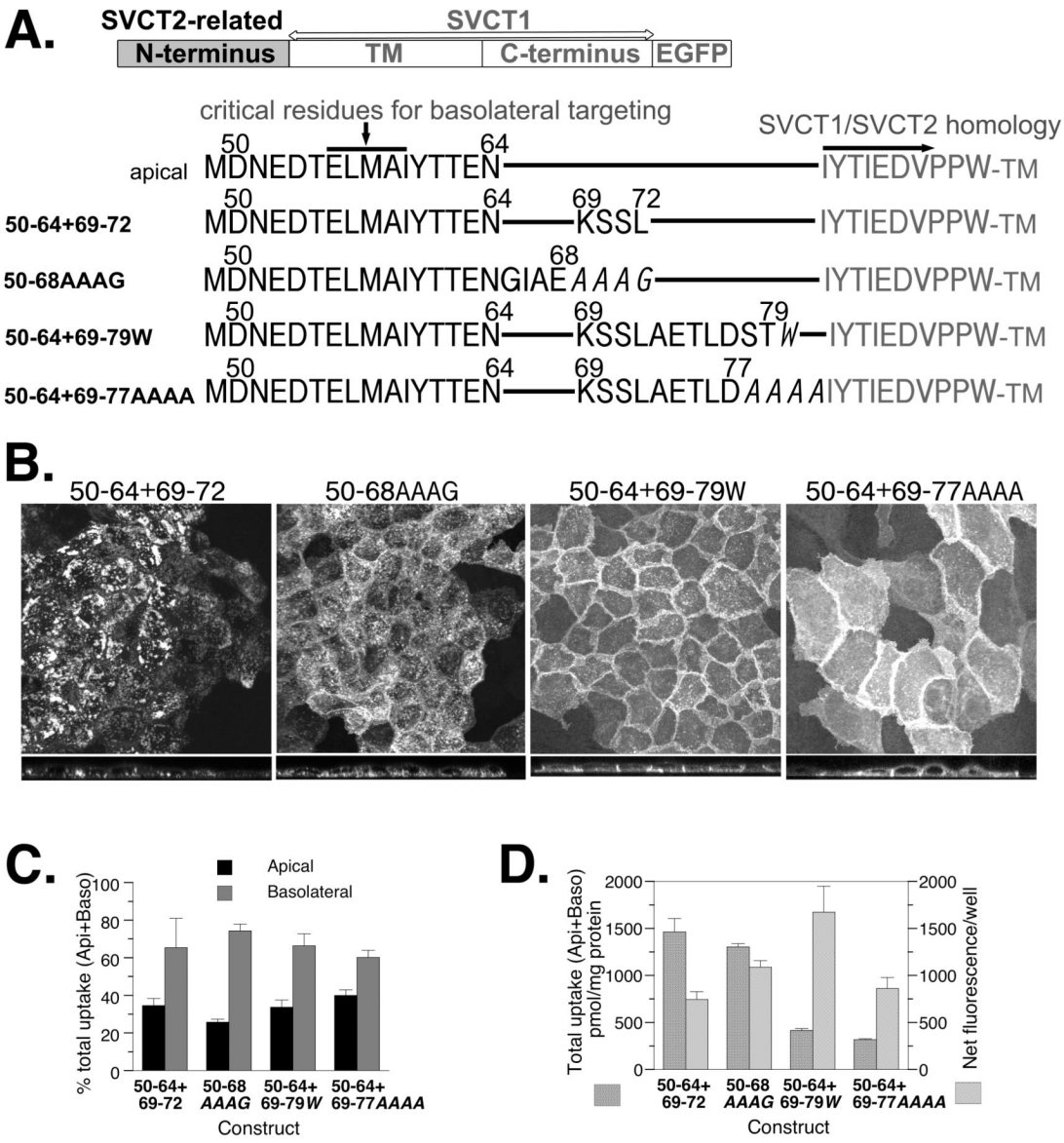

FIGURE 3.

The effects of length and sequence fidelity of SVCT2 N-terminal sequence in its ability to target SVCT1 to the basolateral membrane of well-differentiated MDCK cells. (A) Schematic and sequence presentation of homologous chimeras containing SVCT2-related N-terminal sequence linking to SVCT1 sequence without any SVCT1-specific N-terminal sequence. Amino acid residues in italics represent mutated residues not found in the native SVCT2 N-terminus. (B) Representative confocal merged XY and YZ images of well-differentiated MDCK cells stably expressing each construct. (C) The proportion of ascorbate uptake across the apical (Api) and basolateral (Baso) membrane of MDCK cells stably expressing each construct and grown on Transwells. (D) The efficiency with which each construct was incorporated into the cell membrane. (C,D) Data shown are means±SD of triplicate wells. Some error bars are too small to be visible.

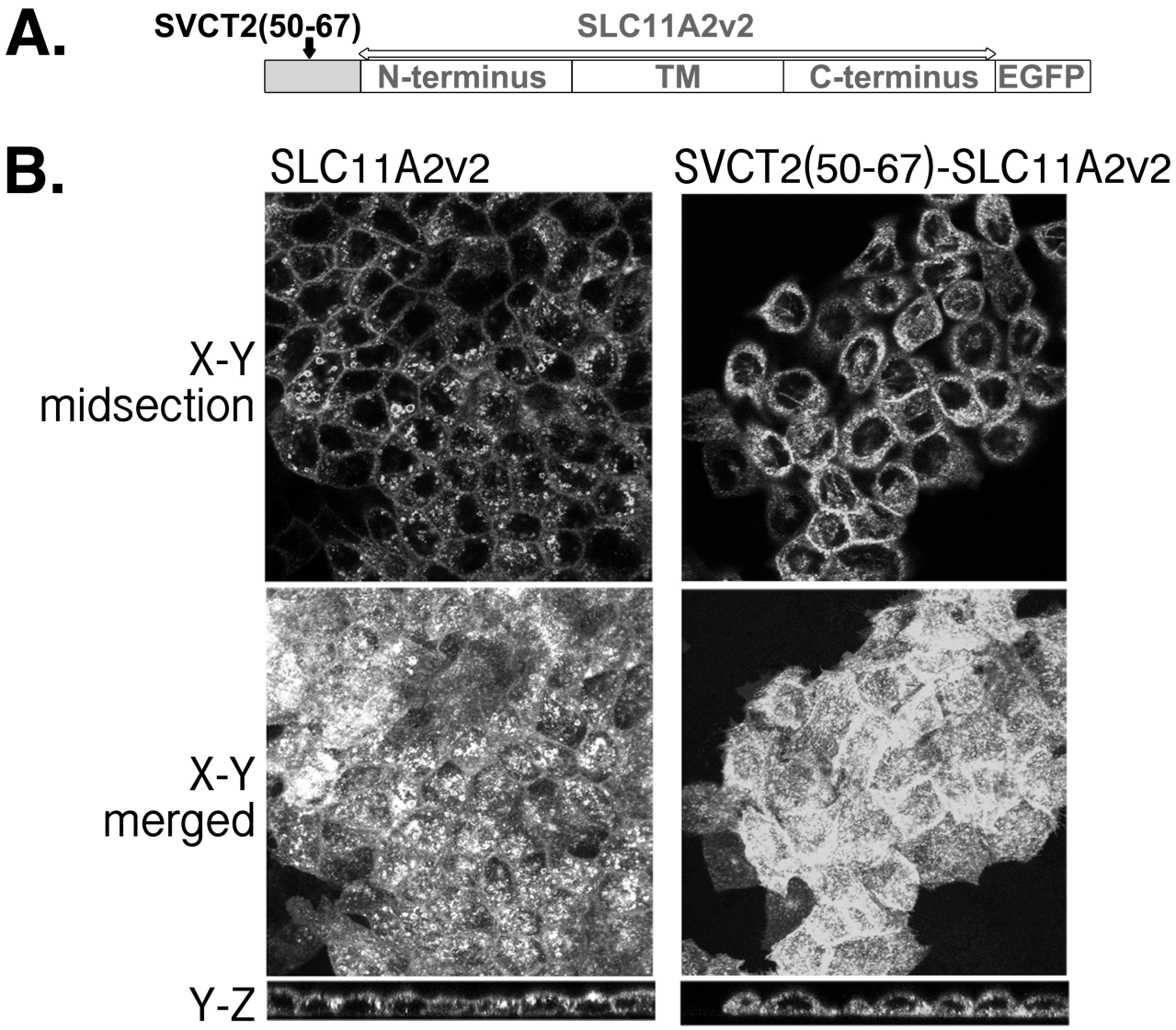

FIGURE 4.

The effect of SVCT2 N-terminal residues on the targeting of SLC11A2v2 in well-differentiated MDCK cells. (A) Schematic presentation of the heterologous chimera pSVCT2(50-64)-SLC11A2v2; (B) (Left) Representative confocal images of MDCK cells stably expressing pSLC11A2v2-EGFP. (Right) Representative confocal images of MDCK cells stably expressing the heterologous chimera, pSVCT2(50-64)-SLC11A2v2-EGFP.

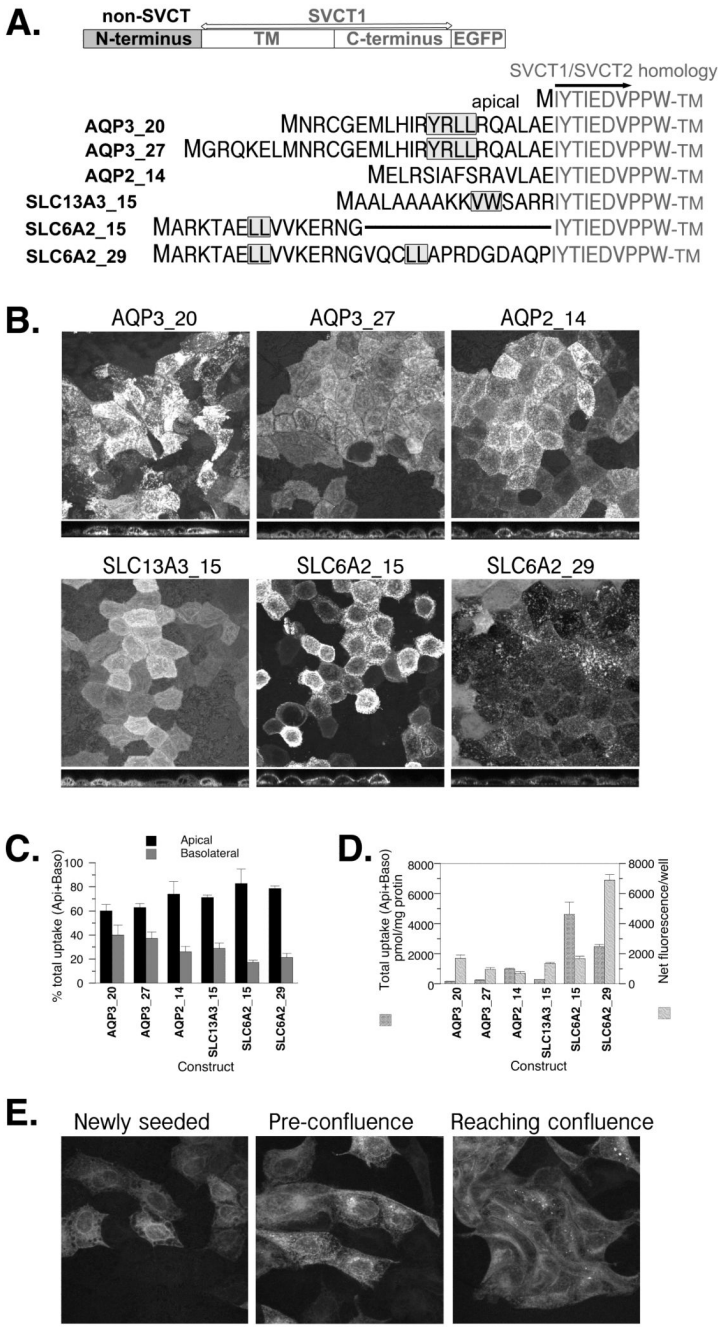

FIGURE 5.

The effects of N-terminal sequences from other multipass membrane proteins, AQP3, AQP2, SLC13A3 and SLC6A2, on the localization of SVCT1 in well-differentiated MDCK cells. (A) Schematic and sequence presentation of heterologous chimeras containing N-terminal sequence from the protein indicated linking to SVCT1 sequence without any SVCT1-specific N-terminal sequence. Numbers after the protein names represent the length of N-terminus included in the chimera. AQP3_20 had residues 9-28 of AQP3 inserted while AQP3_27 had the entire AQP3 N-terminus. AQP2_14 had residues 3-16 of the 15 unique residues in the AQP2 N-terminus inserted. SLC13A3_15 had all 15 unique residues of SLC13A3 N-terminus inserted. Wildtype SLC6A2 has 61 residues in the N terminus after

the initiating methionine. SLC6A2_15 had residues 27-41 inserted and SLC6A2_29 had residues 27-55 inserted. Shaded amino acid residues represent residues previously shown to be critical for the basolateral targeting of parental protein (6-8). (B) Representative confocal merged XY and YZ images of MDCK cells stably expressing each construct. (C) The proportion of ascorbate uptake across the apical (Api) and basolateral (Baso) membrane of MDCK cells stably expressing each construct and grown on Transwells. (D) The efficiency with which each construct was incorporated into the cell membrane. (C,D) Data shown are means±SD of triplicate wells. Some error bars are too small to be visible. (E) The localization of SLC13A3_15 in subconfluent MDCK cells.

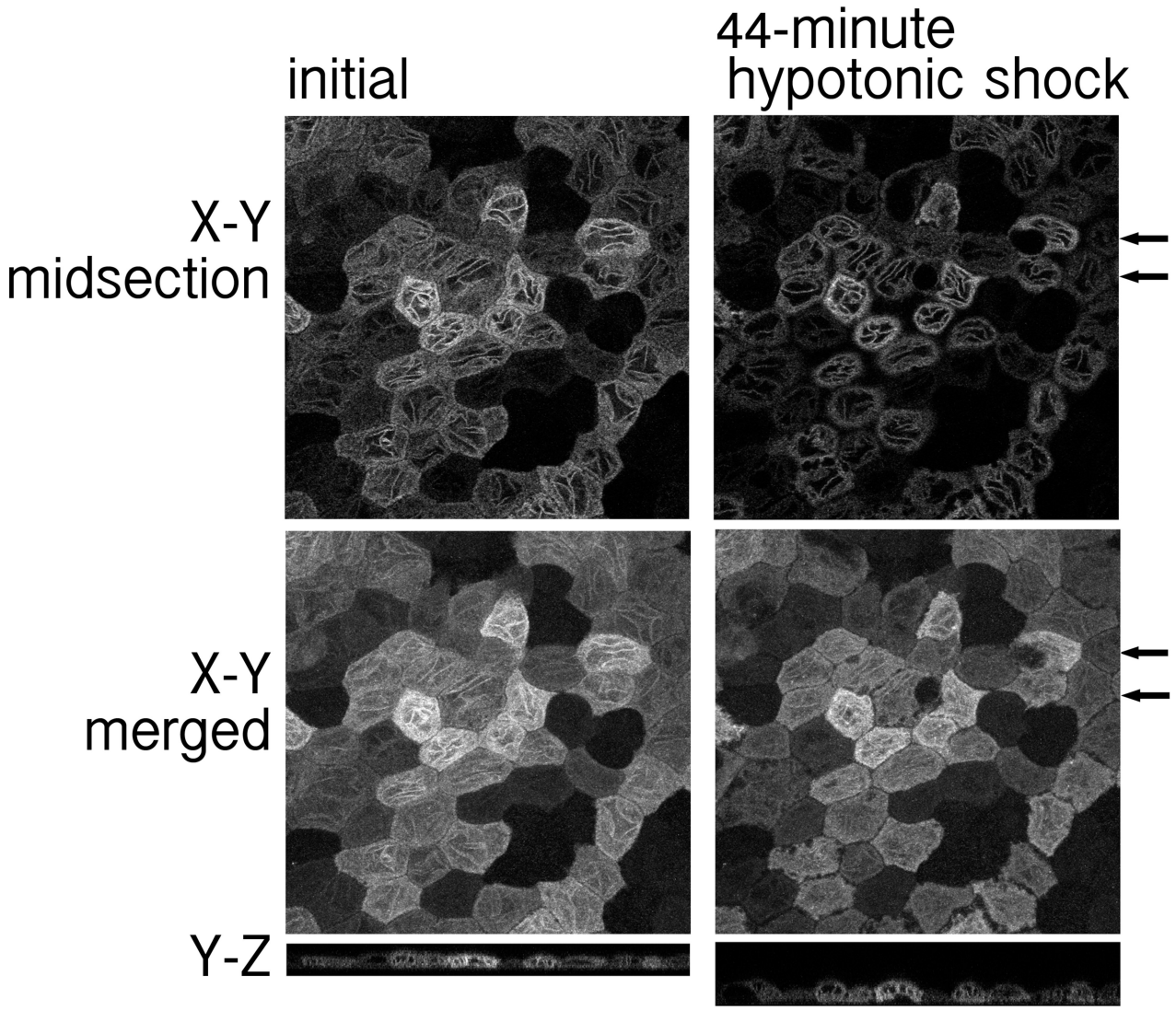

FIGURE 6.

The linear fluorescent tubulin-like structure (TLS) found in well-differentiated MDCK cells expressing SLC13A3_15 persisted after a 44-minute hypotonic shock. (Left) Images of XY midsection and merged XY and YZ sections in Hanks' balanced salt solution with 0.5% FBS. (Right) Images of XY midsection and merged XY and YZ sections of cells treated with 25% osmolarity hypotonic shock at 37° C incubation for 44-minute. Hypotonic condition was created by adding 1.5 ml sterile water to the 0.5 ml Hanks' balanced salt solution with 0.5% FBS in the chamber. Arrows: the location of cells that became deformed during the shock.

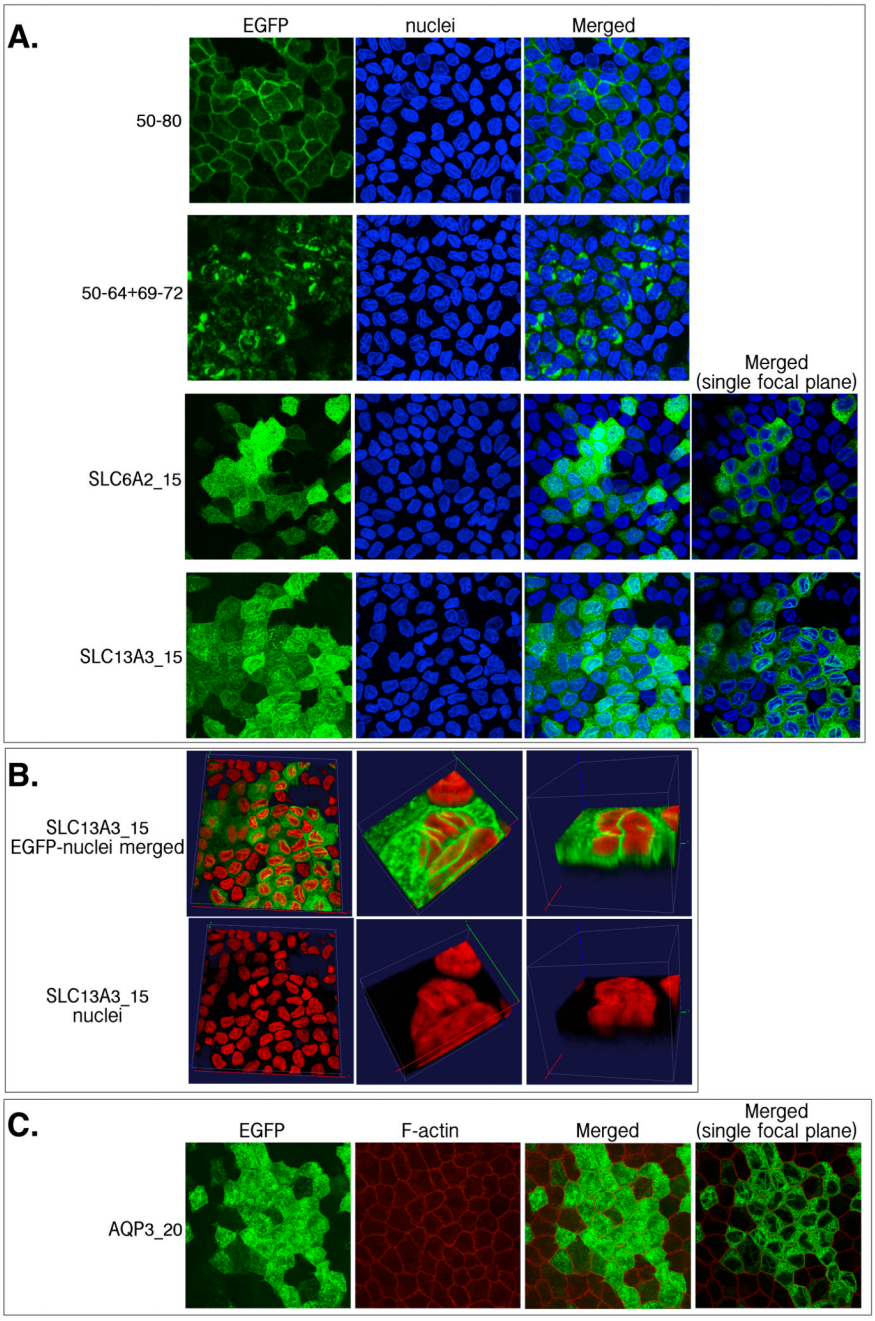

FIGURE 7.

A comparison between the location of EGFP-tagged proteins and nuclei, stained with DAPI (A, B); F-actin, stained with Alexa Fluor® 568-tagged phalloidin (C), in stably-transfected well-differentiated MDCK cells. Cells were briefly fixed with ice-cold 100% methanol and then stained by DAPI or phalloidin immediately for confocal visualization of fluorescence. (B) Enlarged 3-D viewing of DAPI-stained cells to visualize the distribution of linear fluorescence structure around nuclei.

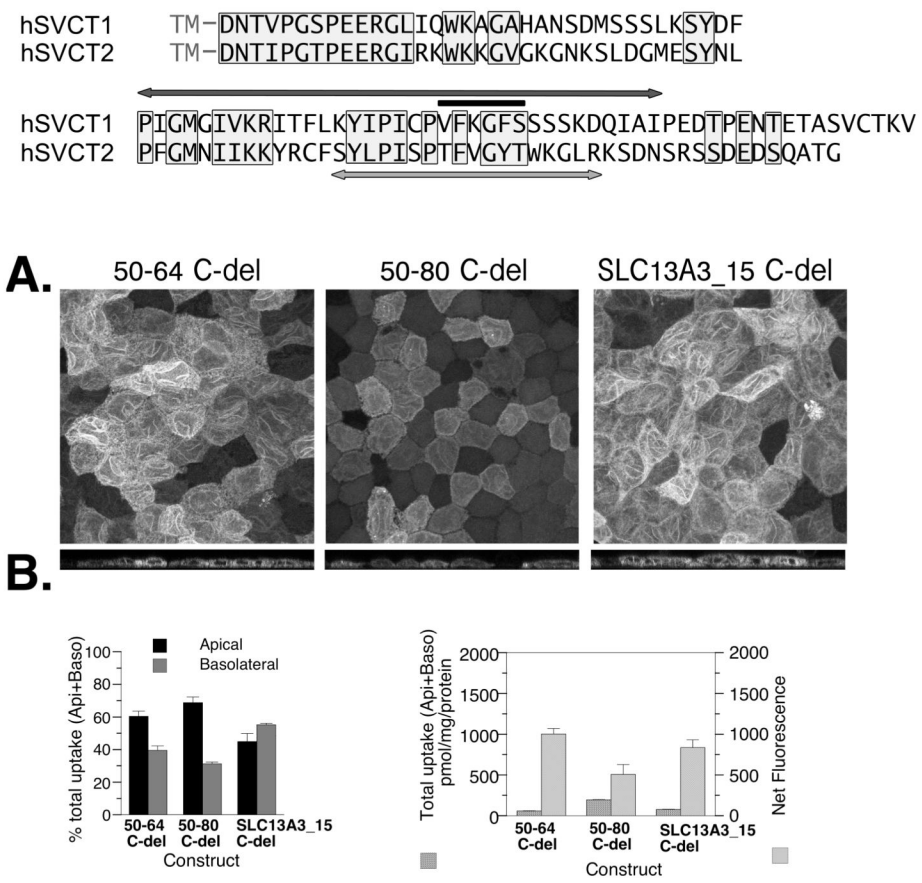

FIGURE 8.

The effect of C-terminal truncation on the localization of three chimeric proteins, apically localized 50-64, basolaterally localized 50-80, and SLC13A3_15 with TLS. (A) Alignment of the C-termini of hSVCT1 and hSVCT2. The sequence within the light-grey box represents homology. The hSVCT1 residues under the black line were shown to be critical for apical localization of hSVCT1 (44). The hSVCT2 residues above the light-grey arrow were shown to be critical for membrane localization of both apical and basolateral SVCT proteins (4). The hSVCT1 residues beneath the darkgrey arrow were removed in the three constructs tested in this figure. (B) The TLS is visible for all three constructs in the confocal merged XY and YZ images. (C) The proportion of ascorbate uptake across the apical (Api) and basolateral (Baso) membrane of well-differentiated MDCK cells stably expressing each construct and grown on Transwells. (D) The efficiency with which each chimeric protein is incorporated into the cell membrane. (C,D) Data shown are means±SD of triplicate wells. Some error bars are too small to be visible.

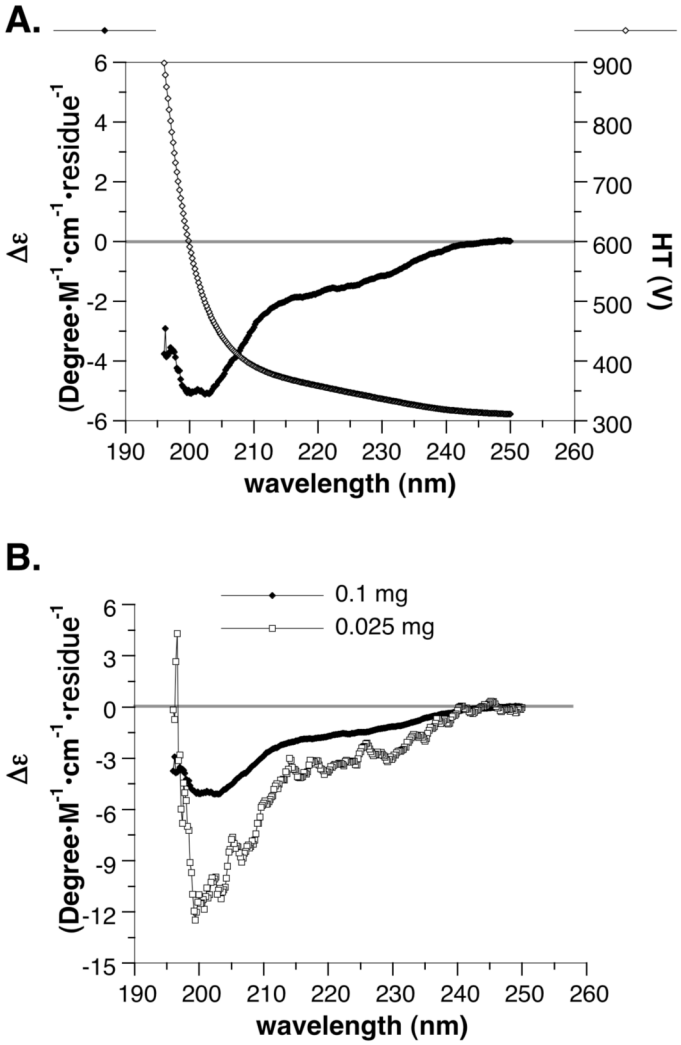

FIGURE 9.

The CD spectrum of hSVCT2 N-terminus (residues 13-89). (A) The Δε and high-tension voltage (HT) of 100 μg peptide/ml phosphate buffer are plotted against wavelength; (B) The Δε plots of 100 and 25 μg peptide/ml phosphate buffer are compared. The spectrum does not predict the presence of α-helix.

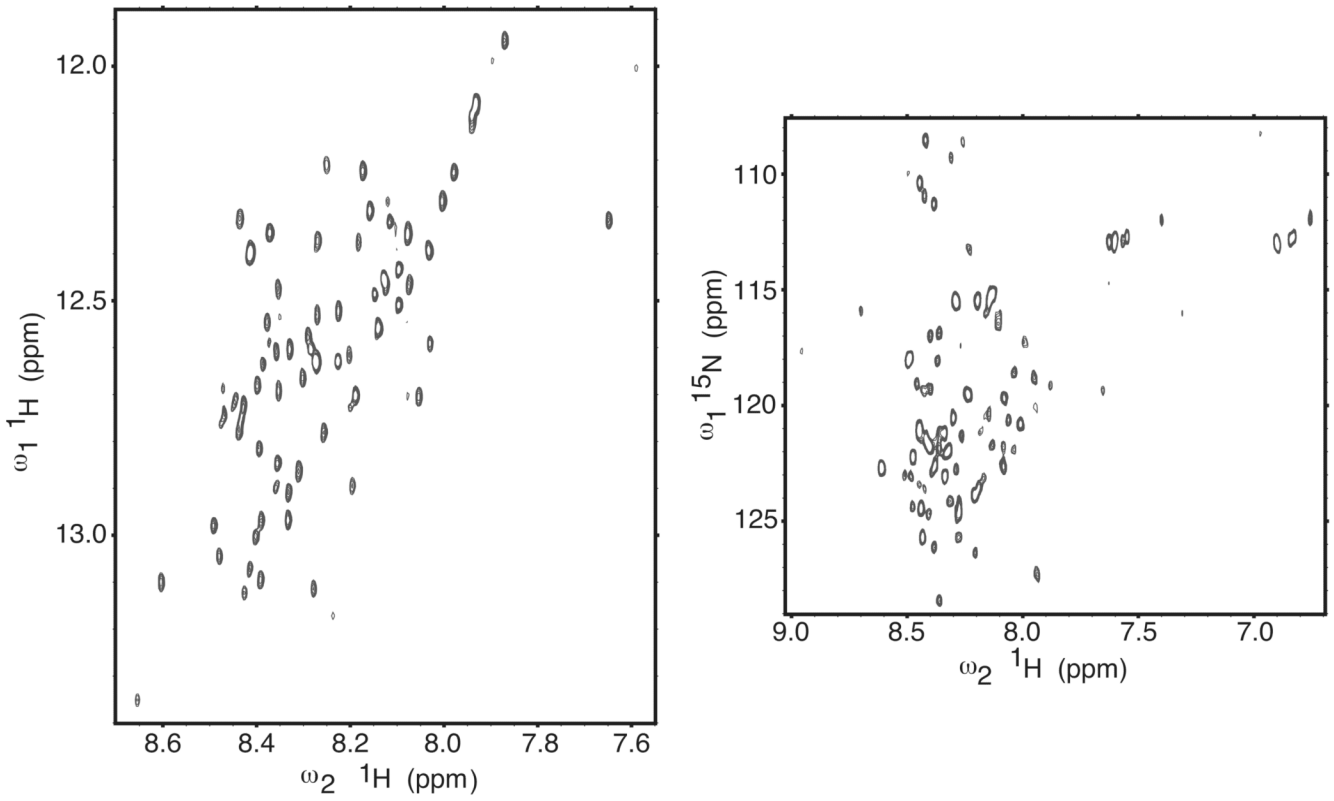

FIGURE 10.

The 2D NMR spectra of the hSVCT2 N-terminus (residues 13-99). Protein sample was at 0.5 mM concentration, pH 7.0, and 295 K (no isotope labeling); data collected at 600 MHz on a non-cryogenic probe. Left panel: ^{N}H-$^{\alpha}H$ region of a homonuclear 2-quantum COSY spectrum (the peaks are anti-phase doublets in the directly detected dimension, but for clarity only the positive contour levels are drawn). The horizontal axis shows the ^{N}H shifts, and the vertical axis shows the sum of the ^{N}H and $^{\alpha}H$ shifts. Right panel: HSQC spectrum for the natural abundance ^{15}N-^{1}H and ^{15}N-$^{1}H_2$ groups.

Table 1

Sequences of PCR primers used in the study.

Mutant	forward primer[a] or primer pairs[b] (5′ to 3′)
Insertion of SVCT2 N-terminal residues into the N-terminus of hSVCT1 [c]	
45-64	GCCTAAGTTTGACATGAGCAGCGGTGAGCAGGACAACGAGGAC
50-72	AAAAGCAGCCTGATTTACAAGATAGAGGACGTGCCACC TTCCGCAATCCCGTTCTCGGTGGTGTAAATCGCC
45-72	GCCTAAGTTTGACATGAGCAGCGGTGAGCAGGACAACGAGGAC
50-80	TCAACTGGGATTTACAAGATAGAGGACGTGCCACC ATCCAGTGTTTCCGCCAGGCTGCTTTTCTCCGC
50-68+AAAG	GCAGCAGCAGCCATTTACAAGATAGAGGACGTGCCACC TTCCGCAATCCCGTTCTCGGTGGTGTAAATCGCC
50-64+69-79+W	TCAACTGGGATTTACAAGATAGAGGACGTGCCACC ATCCAGTGTTTCCGCCAGGCTGCTTTTGTTCTCGG
50-64+69-77+AAAA	GCAGCAGCAGCCATTTACAAGATAGAGGACGTGCCACC ATCCAGTGTTTCCGCCAGGCTGCTTTTGTTCTCGG
Primer pair for C-terminal deletion mutation [d]	
C-del(Δ547-581of SVCT1)	CCAGAAGACACTCCAGAAAATACAGAAAC GAAATCGTAGCTCTTGAGGCTGGAAG
Primer pairs for inserting heterologous N-terminus [e]	
AQP3_20	TACAGACTACTTCGCCAGGCTTTAGCAGAGATTTACAAGATAGAGGACGTGCCACC CCGTATGTGTAGCATTTCTCCGCAACGATTCATGTCAAACTTAGGCTCTGTGGG
AQP3_27	AAAGAGTTGATGAATCGTTGCGGAGAAATGCTAC CTGTCTTCCCATGTCAAACTTAGGCTCTGTGG
AQP2_14	AGTCGTGCTGTGTTTGCCGAGATTTACAAGATAGAGGACGTGCCACC AAAAGCAATAGAACGCAACTCCATGTCAAACTTAGGCTCTGTGG
SLC13A3_15	GCTAAGAAAGTTTGGTCTGCTCGGAGGATTTACAAGATAGAGGACGTGCCACC AGCAGCAGCGAGTGCCGCCATGTCAAACTTAGGCTCTGTGGG
SLC6A2_15	GTAGTCAAAGAGAGGAATGGTATTTACAAGATAGAGGACGTGCCACC CAATAACTCTGCCGTCTTGCGTGCCATGTCAAACTTAGGCTCTGTGGG
SLC6A2_29	CGTGATGGAGATGCTCAACCGATTTACAAGATAGAGGACGTGCCACC AGGGGCTAATAAACACTGAACACCATTCCTCTCTTTGACTACCAATAACTCTG
Primer pairs for constructing additional plasmids [f]	
His-SVCT2 (13-89)	ATAAGCTTACTACATGTCTGATCGCTGGGG AAGAATTCGACGACGACGACAAGGCTAGCATGGAGGCTGGAAGTTCAAC
His-SVCT2 (13-99)	GATGTTCCTCCTTGGTAGTAAGCTTGGCACTGGCCG CTCAATGGTGTAGAGCATGTCTGATCGCTGGGG
SLC11A2v2	AAGCTAGCCATGGTGTTGG CCTTTGTAGATGTCCACAGCC
SVCT2(50-67)-SLC11A2v2	CTAGCCATGGACAACGAGGACACCGAGCTGATGGCGATTTACACCACCGAGAACGGG GGTACCTGTTGCTCCTGTGGCTCGACTACCGCTAAATGTGGTGGCTCTTGCCCGATC

[a] For insertion mutations that used Stratagene Quik-Change site-directed mutagenesis kit, a pair of complementary primers were used.

[b] For insertion mutations that used Finnzymes Phusion site-directed mutagenesis kit, sense and antisense primers were used.

[c] Residues were inserted into hSVCT1Δ1-30 (N-terminal deletion mutant of hSVCT1 with only N-terminal residues that are identical to that of hSVCT2 (4)) after the initiating methionine. Numbers shown are the position of amino acid residues in the wildtype hSVCT2 N-terminus. Letters shown after the numbers represent the additional mutated sequence inserted.

[d] Numbers shown are the position of amino acid residues in the C-terminus of wildtype hSVCT1. These residues were deleted from several chimera constructs.

[e] N-terminal sequence of each protein was inserted into hSVCT1Δ1-30 after the initiating methionine. Numbers shown are the number of N-terminal residues from each wildtype protein.

[f] N-terminal residues of hSVCT2 were inserted into constructs for expression or for functional study. Numbers in the parenthesis represent the position of N-terminal residues in the wildtype hSVCT2.